

# MODEL PREDICTIVE CONTROL OF FEED FLOW REVERSAL IN A REVERSE OSMOSIS DESALINATION PROCESS

Alex R. Bartman, Charles W. McFall, Panagiotis D. Christofides and Yoram Cohen

**Abstract**—Model-predictive control algorithms are applied to a high capacity reverse osmosis (RO) membrane desalination process simulation that utilizes feed flow-reversal in order to prevent and/or reverse scale crystal formation on the membrane surface. A dynamic non-linear model which incorporates feed concentration and membrane properties is used for simulation and demonstration of optimally controlled feed flow reversal. Before flow reversal can take place on a high capacity RO plant, the flow into the membrane unit must be carefully reduced to eliminate the risk of membrane module damage and unnecessary energy consumption. A cost-function is formulated for the transition between the normal high flow steady-state operating point to a low flow steady-state operating point where it is safe to reverse the flow direction. Open-loop and closed-loop simulations demonstrate non-linear model-predictive control strategies that induce transition from the high-flow to low-flow steady-states in an optimal way.

## I. INTRODUCTION

Reverse osmosis (RO) membrane desalination has emerged as one of the leading methods for water desalination due to the low cost and energy efficiency of the process [19]. Lack of fresh water sources has necessitated further development of these desalination plants, especially in areas with dry climates. In many reverse osmosis processes, particularly with brackish water feeds or processes running at a high level of recovery, dissolved ions can precipitate out of solution and crystallize on the membrane surface in a process called scaling. Scale formation on the membrane surface will lead to decreased permeate productivity [9], as well as permanent membrane damage if scaling is allowed to progress past its initial stages.

Several methods are currently used to prevent scale formation; addition of anti-scalant chemicals to the feed or flushing the membrane units with low-TDS (total dissolved solids) permeate water. These current methods of scale mitigation have several disadvantages. Anti-scalants are only useful to a degree, and if added in excess, may actually promote scaling or fouling [20]. The cost of the anti-scalant compounds is also an important consideration [4]. In the case of the permeate flush, this process will require the reverse osmosis operation to stop for a substantial amount of time to allow for the flushing cycle, eliminating any permeate production (even using up some of the previously produced permeate water). To deal with these issues, a novel technique called feed

flow reversal has been developed, which can prevent scale formation without the addition of expensive chemicals or extensive periods of system down-time [18]. This technique uses a system of solenoid valves around the membrane modules configured specifically so that the direction of the feed flow through the membrane units can be reversed (see Fig. 1). This reversal of the feed flow also reverses the axial salt concentration profile [8] at the surface of the membrane, effectively “resetting the induction clock”, where induction refers to the amount of time before scale crystals begin to form on the membrane surface [18]. The reversal, if activated after crystals have already been formed, also allows the dissolution of a substantial portion of scale deposited on the membrane surface.

It is imperative to operate the flow reversal process for the correct length of time; switching back to normal flow too quickly may leave scale crystals on the membrane (and in the case where scale crystals have not formed yet, the induction clock will not “reset”), while operating the flow reversal for too long may cause scale to form on the outlet end of the membrane surface. Several techniques can be employed to determine if scale has formed; measurements of the permeate flow can be monitored to determine if flux decline has occurred, or a novel method such as the EX-situ Scale Observation Detector (EXSOD) system can be used [21]. With the latter method, scale crystals can be detected before flux decline occurs via automated image analysis software (currently under development by the authors); this algorithm is also able to trigger the switch between normal flow and flow reversal mode.

When operating a system that utilizes feed flow reversal, it is important to carry out the mode switching (from forward flow to reverse flow) in a manner which will not cause water hammer. The phenomenon of water hammer takes place when fluid moving at a moderate to high velocity ( $velocity > 1.5 \frac{m}{s}$  for the example in this work) suddenly encounters a blockage in the pipe (for instance, when a solenoid valve is instantly closed). The fluid’s inertia causes it to slam into the blockage, causing a pressure wave and often wear/damage to the process equipment [10]. The Joukowski formula [17] can be used to estimate the magnitude of the pressure wave caused by water hammer for a given system configuration, and it is seen that this problem can be especially prominent in large systems with a high feed flow rate.

For example, consider the system presented in Fig. 2. Initially solenoid valves  $s_2$  and  $s_3$  are closed and  $s_1$  and  $s_4$  are open. Furthermore, the velocity entering the membrane unit,

Department of Chemical and Biomolecular Engineering University of California, Los Angeles, CA 90095. Corresponding author is P. D. Christofides [pdc@seas.ucla.edu](mailto:pdc@seas.ucla.edu)

Financial support from the National Science Foundation, CTS-0529295, and the State of California Department of Water Resources is gratefully acknowledged.

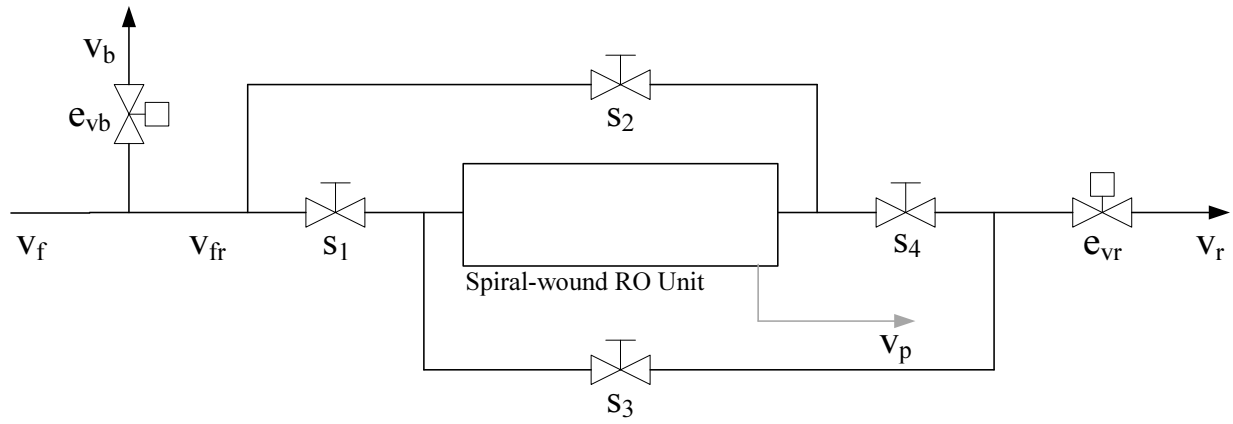


Fig. 1. An expanded view of the flow reversal configuration surrounding the spiral-wound unit

$v_{fr}$ , is  $10 \frac{m}{s}$ . When flow reversal is initiated, solenoid valves  $s_2$  and  $s_3$  are opened and assuming similar flow resistance in each path, the flow splits approximately evenly through the three possible paths. The stream velocities through  $s_2$ ,  $s_3$ , and the membrane unit are approximately  $3.3 \frac{m}{s}$ . However, the stream velocities going through  $s_1$  and  $s_4$  are approximately  $6.7 \frac{m}{s}$ . With a maximum velocity threshold of  $1.5 \frac{m}{s}$ , none of these flow velocities are low enough to enable the closure of a solenoid valve without the possibility of causing component damage through water hammer. From this example, it is clear that with the configuration seen in Fig. 2, water hammer is of concern when the velocity into the membrane units is approximately 1.5 times the water hammer threshold.

Motivated by these considerations, the goal of this work is to use model-predictive control (MPC) to determine the optimal switching path from normal operating conditions to a condition where the stream velocity entering the membranes is much lower; preventing water hammer during solenoid valve closure while avoiding pressure fluctuations and decreased process performance during the transition. Alleviating these phenomena will prolong equipment life-span and help to maximize the productivity of the RO system. The formulation presented in this work is specific to the system presented in Fig. 2, but it is important to note that these MPC algorithms can be adapted to any flow-reversal equipped reverse osmosis system where the operator is able to control the stream velocity entering the membrane units. Model-predictive control has not been employed for use with the feed flow reversal technique, but has been evaluated for the overall control of RO desalination processes [1]. It is noted that in a recent work [12], Lyapunov-based non-linear control systems and model-based monitoring schemes were designed for fault-tolerant control of RO processes in the presence of actuator faults without dealing with the issue of optimization of the feed flow reversal process. Optimization with MPC requires the use of a RO desalination system model, which has been derived based on mass and energy balances [13]. A cost function that takes into account control action, stream velocities, and system pressure is proposed,

along with several hard process constraints which represent physical limitations of the system. The model, cost function, and constraints are arranged into a non-linear optimization problem which is solved through the use of a numerical optimization algorithm. Closed-loop simulations with MPC are performed in this work to demonstrate the mode switching dynamics.

## II. RO SYSTEM MODEL

As seen in Fig. 2, feed water enters the system and is pressurized by the high-pressure pump. The pressurized stream is split into a bypass stream (with velocity  $v_b$ ) and the stream which enters the spiral-wound membrane unit(s) ( $v_{fr}$ ). Two streams also exit the membrane module, the retentate (or brine) stream, with velocity  $v_r$ , and the permeate stream.

The model derivation is based on an overall mass balance and local energy balances around the valves of the system [13]. In the model derivation, it is assumed that the water is incompressible, all components are operated on the same plane (potential energy terms due to gravity are neglected), and the density of the water is assumed to be constant. It is also assumed that the effective concentration in the RO unit is a weighted average of the feed and retentate concentrations (Eq. 4).

The model derivation results in two non-linear ordinary differential equations (ODEs), along with an algebraic expression for system pressure. An equation for the osmotic pressure based on the temperature and effective concentration in the membrane unit was developed in [11], and is used as an estimate for various solutions. Specifically, the model has the following form:

$$\frac{dv_b}{dt} = \frac{A_p^2}{A_m K_m V} (v_f - v_b - v_r) + \frac{A_p}{\rho V} \Delta\pi - \frac{1}{2} \frac{A_p e_{vb} v_b^2}{V} \quad (1)$$

$$\frac{dv_r}{dt} = \frac{A_p^2}{A_m K_m V} (v_f - v_b - v_r) + \frac{A_p}{\rho V} \Delta\pi - \frac{1}{2} \frac{A_p e_{vr} v_r^2}{V} \quad (2)$$

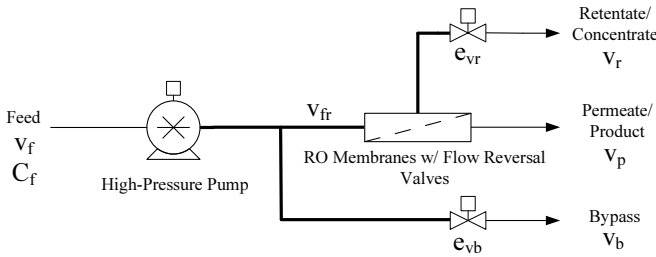


Fig. 2. Overall reverse osmosis system diagram

$$\Delta\pi = \delta C_{eff}(T + 273) \quad (3)$$

$$C_{eff} = C_f \left( a + (1-a) \left( \frac{(1-R) + R(v_f - v_b)}{v_r} \right) \right) \quad (4)$$

$$P_{sys} = \frac{\rho A_p}{A_m K_m} (v_f - v_b - v_r) + \Delta\pi \quad (5)$$

where  $\rho$  is the fluid density,  $V$  is the system volume,  $v_f$  is the feed velocity,  $A_p$  is the pipe cross-sectional area,  $A_m$  is the membrane area,  $K_m$  is the membrane overall mass transfer coefficient,  $C_f$  is the amount of total dissolved solids (TDS) in the feed,  $C_{eff}$  is the effective average concentration at the membrane surface,  $a$  is an effective concentration weighting coefficient,  $\Delta\pi$  is the difference in osmotic pressure between the feed side of the membrane and the permeate side,  $\delta$  is a constant relating effective concentration to osmotic pressure,  $v_b$  is the bypass flow velocity,  $v_r$  is the retentate flow velocity,  $P_{sys}$  is the system pressure,  $R$  is the fractional salt rejection of the membrane,  $e_{vb}$  is the bypass valve resistance, and  $e_{vr}$  is the retentate valve resistance. Using these dynamic equations, various control techniques can be applied using the valve resistance values as the manipulated inputs ( $e_{vb}, e_{vr}$ ). As the valve resistance goes to zero, the valve behaves as an open pipe; as the valve resistance approaches infinity, the valve behaves as a total obstruction and the flow velocity goes to zero [3].

In order to accurately model the valve dynamics and obtain practical constraints, the concept of valve  $C_v$  is used. The definition of  $C_v$  for a valve in a water system is presented in Eq. 6, where  $Q$  is the volumetric flow rate through the valve.

$$C_v = \frac{Q}{\sqrt{P_{sys}}} \quad (6)$$

Using a simplified energy balance around one valve:

$$\frac{dv}{dt} = \frac{P_{sys} A_p}{\rho V} - \frac{1}{2} \frac{A_p e_v v^2}{V} \quad (7)$$

Steady state is assumed, and the simplified energy balance is rearranged to yield:

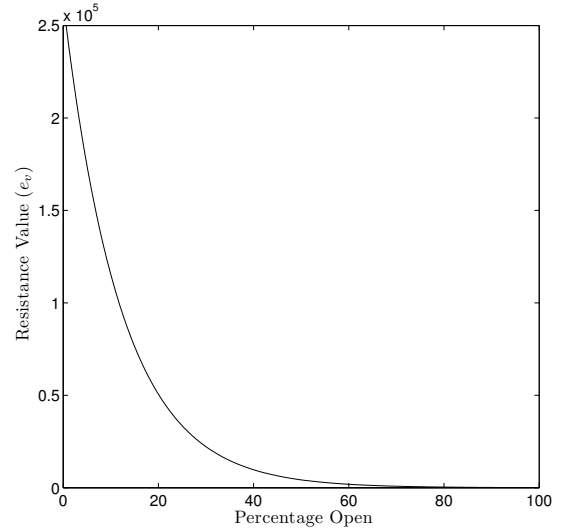


Fig. 3. Valve resistance values ( $e_v$ ) vs. valve position

$$C_v = \frac{1}{A_p \sqrt{\frac{1}{2} \rho e_v}} \quad (8)$$

Depending on the type of valve and its flow characteristics, it is assumed that the  $C_v$  value (and in turn, the  $e_v$  values from the model) can be related to the valve position (percentage open) through the following empirical logarithmic relation based on commercially available valve data:

$$O_p = \mu \ln \left( \frac{1}{A_p \sqrt{\frac{1}{2} \rho e_v}} \right) + \phi \quad (9)$$

where  $\mu$  and  $\phi$  are constants depending on the valve properties. For the model presented in this paper, the curve relating valve position ( $O_p$ ) to resistance value ( $e_v$ ) is shown in Fig. 3. It can be seen in Fig. 3 that as the valve position goes to zero (fully closed), the valve resistance values begin to grow at an increasing rate; and as the valve approaches the fully-open position, the resistance values change slowly. This treatment of the valve characteristics allows for constraints based on valve actuator speed to be incorporated into the RO system model and into the controller calculations.

### III. MODEL PREDICTIVE CONTROL OF FLOW REVERSAL

When switching the system into flow-reversal mode, it is desired to bring the feed velocity into the membranes ( $v_{fr}$ ) below the velocity threshold; where the flow will not cause significant water hammer when the solenoid valves are closed. In order to decrease the membrane feed velocity ( $v_{fr}$ ), it will be necessary to open the bypass valve. It is desired to keep the system pressure constant while decreasing the velocity so that the membrane and system components will not be damaged. This can be done by closing the

TABLE I  
PROCESS PARAMETERS AND NORMAL MODE STEADY-STATE VALUES  
(*nss*)

$\rho$	=	1000	$kg/m^3$
$V$	=	0.04	$m^3$
$v_f$	=	10	$m/s$
$A_p$	=	1.27	$cm^2$
$A_m$	=	30	$m^2$
$K_m$	=	$9.218 \times 10^{-9}$	$s/m$
$C_f$	=	10000	$mg/L$
$a$	=	0.5	
$T$	=	25	$^{\circ}C$
$R$	=	0.993	
$\mu$	=	24.270	
$\phi$	=	153.554	
$\delta$	=	0.2641	$Pa/(ppm * K)$
$v_b^{nss}$	=	1.123	$m/s$
$v_r^{nss}$	=	4.511	$m/s$
$P_{sys}^{sp}$	=	457.51	$psi$
$e_{vb}^{nss}$	=	5000	
$e_{vr}^{nss}$	=	310	

retentate valve while the bypass valve is being opened, in such a fashion that the system pressure fluctuates less than a pre-defined tolerance. MPC is used to complete this transition in an optimal way.

When reversing the flow, the solenoid valves ( $s_i$ ), arranged as seen in Fig. 1, are opened/closed in a specific sequence. First, valves  $s_2$  and  $s_3$  are opened, then valves  $s_1$  and  $s_4$  are closed. After these actions are completed, the retentate and bypass valves can be manipulated to return the process to the desired steady state. The normal steady state operating point is used as the initial condition for the mode switching. To determine the final state after mode switching, the procedure is as follows: Using the normal steady state operating point, the pressure set point is calculated using Eq. 5. In this case,  $P_{sys}^{sp} = 457.51$  psi. Second, setting the bypass velocity to  $v_f - 1.5 \frac{m}{s}$  (equivalent to setting  $v_{fr} = 1.5 \frac{m}{s}$ ) and using the desired pressure set point, the low-flow steady state operating point value for  $v_r^{lss}$  can be determined. With the steady state values of  $v_r^{lss}$ ,  $v_b^{lss}$ , and the pressure set point  $P_{sys}^{sp}$ , the model equations can be solved for the valve resistance values  $e_{vb}^{lss}$  and  $e_{vr}^{lss}$  corresponding to the low-flow operating point. Following this procedure, the low-flow steady state operating point is known, but the optimal path taken to get there from the initial operating steady state is not.

While it is desired to complete this flow direction switching with minimal impact on the system pressure, and in the shortest time possible, it is also necessary to factor in several system parameters such as pressure variation allowed, the bypass stream velocity as compared to the water hammer threshold, and the amount of control energy expended. To account for these issues, an optimization cost function is first proposed:

$$C(x, x_0, u) = \sum_{i=n_c}^{n_c+N} \left[ \alpha \left( \frac{P_{sys}(i)}{P_{sys}^{sp}} - 1 \right)^2 + \beta \left( \frac{v_{fr}(i)}{v_{wh}} - 1 \right)^2 + \gamma \left( \left( \frac{e_{vb}(i)}{e_{vb}^{lss}} - 1 \right)^2 + \left( \frac{e_{vr}(i)}{e_{vr}^{lss}} - 1 \right)^2 \right) \right] \quad (10)$$

where  $n_c$  is the current time-step,  $n_c + N$  is the current time-step plus the prediction horizon, and  $v_{wh}$  is the water hammer threshold velocity. The prediction horizon,  $N$ , is defined such that the optimization is performed from the current time-step to  $N$  time-steps in the future (i.e., from  $t = t_{current}$  to  $t = t_{current} + N t_{step}$ ).

The values of the cost function of Eq. 10 depend on the initial state of the system ( $x_0$ ) and the state of the system between  $t(n_c)$  and  $t(n_c + N)$  (the state,  $x$ , is comprised of  $v_b$  and  $v_r$ ). The cost function also depends heavily on the control actions used ( $u$ ), and weights given to the individual terms by the weighting coefficients  $\alpha$ ,  $\beta$ , and  $\gamma$ . As the optimization procedure is carried out, the optimization algorithm allows for a set of non-linear constraints to be employed. In this formulation, the following two hard actuator constraints are enforced:

$$O_{pi} > 0 \quad (11)$$

$$\left| \frac{dO_{pi}}{dt} \right| \leq R_{valve}^{max} \quad (12)$$

The first constraint forces the valve position values to be positive, since negative values of this variable would be physically meaningless. The second constraint sets a maximum rate of opening/closing for the valves,  $R_{valve}^{max}$ . Additional constraints can be added; constraints on maximum system pressure or other system variables may be desirable for certain types of RO operations.

In order to optimize the constrained transition from normal flow to low-flow and incorporate feedback into the calculation of the control action, a non-linear model-predictive control (MPC) formulation is implemented [5], [6], [15], [16], [7], [14]. In this method, a time frame for the transition is chosen,  $t = 0$  to  $t = t_f$ , along with an optimization time-step  $t_{step}$  and a prediction horizon  $N$ . Using these optimization parameters and the constraints along with the RO system model (with full state feedback) and the cost function weighting parameters  $\alpha$ ,  $\beta$ , and  $\gamma$ , the MPC control scheme can determine an optimal pair of control inputs,  $e_{vb}$  and  $e_{vr}$ , for each time-step.

The MPC optimization involves the following procedure:

- 1) The initial state vector and initial control value guesses are passed to a non-linear optimization algorithm based on sequential quadratic programming;
- 2) The optimization algorithm numerically integrates the model equations from  $t = t_{current}$  to  $t = t_{current} +$

- $Nt_{step}$  using the initial state vector and control value guesses;
- 3) The resulting state vector is used to calculate the value of the cost function;
  - 4) A new set of control inputs are determined, and steps 2-4 are repeated until a minimum cost value is found (i.e.,  $\min_{e_{vb}, e_{vr}} C(x, x_0, u)$ ) subject to the constraints of Eqs. 11 and 12;
  - 5) Optimal control inputs for each  $t_{step}$  are made available to the controller and actuators;
  - 6) Only the first of the optimal control inputs,  $u(t_{current})$ , is applied; the system of Eqs. 1 and 2 is numerically integrated for one time-step (from  $t = t_{current}$  to  $t = t_{current} + t_{step}$ ) using the first optimal control value to yield a new initial state for the next optimization;
  - 7) The remaining optimal control values for the prediction horizon are used as an initial guess for the computation of the control values in the next step;
  - 8) All steps are repeated for each optimization time-step from  $t = 0$  to  $t = t_f - t_{step}$ .

As implicitly stated above, all control values are applied in a sample-and-hold fashion; that is, a control value used in the integration on the interval  $[t_{step_{n-1}} t_{step_n})$  is held constant over the entire interval, and then a new control value is determined by the optimization for the interval  $[t_{step_n} t_{step_{n+1}})$ .

#### IV. SIMULATION RESULTS

##### A. Overview

In order to test the feasibility of MPC for feed flow reversal in a reverse osmosis desalination system, several simulation studies were carried out. Initially, it was desired to examine the effect of using the model-predictive controller to switch between steady states when the process conditions are identical to the nominal plant model. Using a sampling time approximately one tenth of the system step response time, the model-predictive control formulation is applied to the system with various prediction horizons. These simulations are subsequently compared to an “open-loop manually controlled” transition where the control inputs are manipulated to their final values at the maximum rate allowed by the constraints, as well as the case where the transition is controlled using proportional-integral (PI) control. It was also desired to simulate the switching between steady states in the presence of a plant-model mismatch on the feed TDS value. The controller receives state feedback from the plant model at the end of each time-step (i.e., measurements of  $v_b$  and  $v_r$ ), but an offset in system pressure and stream velocity is observed due to the mismatched MPC controller. Simulations are conducted at several prediction horizons, and an integral control input is applied after the MPC reaches steady state in order to bring the system pressure back to the nominal pressure set point. The results of these simulations can be found in the journal paper [2].

TABLE II  
OPTIMIZATION PARAMETERS AND LOW-FLOW MODE STEADY-STATE  
VALUES ( $l_{ss}$ )

$t_0$	=	0	s
$t_{step}$	=	0.1	s
$\alpha$	=	10000	
$\beta$	=	100	
$\gamma$	=	200	
$v_{wh}$	=	1.5	m/s
$v_b^i$	=	1.123	m/s
$v_r^i$	=	4.511	m/s
$C_{feed}^c$	=	10000	ppm
$R_{max}$	=	10	%/s
$v_b^{l_{ss}}$	=	8.5	m/s
$v_r^{l_{ss}}$	=	0.267	m/s
$P_{sys}^{l_{ss}}$	=	457.51	psi
$e_{vb}^{l_{ss}}$	=	87.322	
$e_{vr}^{l_{ss}}$	=	88592	

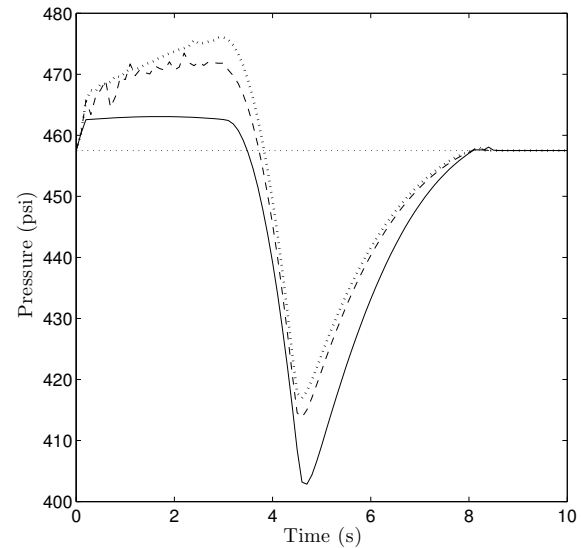


Fig. 4. Steady-state switching using MPC in the absence of plant-model mismatch: system pressure vs. time for  $N=1$  (solid line),  $N=3$  (dashed line), and  $N=5$  (dotted line), including pressure set point (horizontal line)

##### B. Optimal Mode Transition Without Plant-Model Mismatch

As described in the overview, the first simulations demonstrate the switching to low-flow mode using model-predictive control (MPC) in the case where the controller model and plant model are identical. The controller uses measurements of the retentate and bypass stream velocities (system states) and manipulates the valve resistance values. In these simulations, the optimization parameters were set as shown in Table II. Additionally, the system was simulated for 10 seconds ( $t_f$ ), and the prediction horizon,  $N$ , was varied in each simulation. The results are presented in Figs. 4 - 6.

It can be seen that in the valve position and stream velocity plots (Figs. 5 - 6), only a small difference is observed between simulations with various prediction horizons. Even though the difference in control action is slight, a large effect

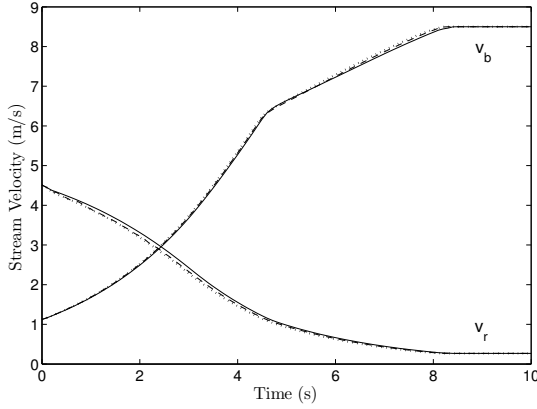


Fig. 5. Steady-state switching using MPC in the absence of plant-model mismatch: retentate and bypass stream velocities vs. time for  $N=1$  (solid line),  $N=3$  (dashed line), and  $N=5$  (dotted line)

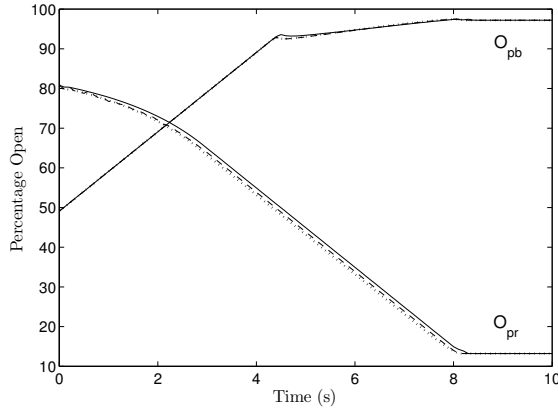


Fig. 6. Steady-state switching using MPC in the absence of plant-model mismatch: valve positions vs. time for  $N=1$  (solid line),  $N=3$  (dashed line), and  $N=5$  (dotted line)

is seen on the system pressure, seen in Fig. 4. In the case of the smallest prediction horizon ( $N = 1$ ), the system pressure drops by approximately 55 psi before returning to the set point. It is seen that as the prediction horizon increases, the maximum deviation from the system pressure set point decreases, showing that the model-predictive control horizon is instrumental in minimizing pressure fluctuations.

The benefits of implementing MPC on the system pressure can be seen even more clearly when the optimized cases are compared to the “open-loop manually controlled” pressure in Fig. 7, where the valves are adjusted to their final steady state at the maximum rate allowable by the constraints. The 100+ psi pressure variation caused by the “open-loop manually controlled” operation should be avoided.

It was also desired to compare the performance of the MPC to proportional-integral (PI) control. Two PI loops were implemented, one loop measuring the bypass stream velocity and using the bypass valve resistance to bring the bypass stream velocity to the water hammer threshold, and

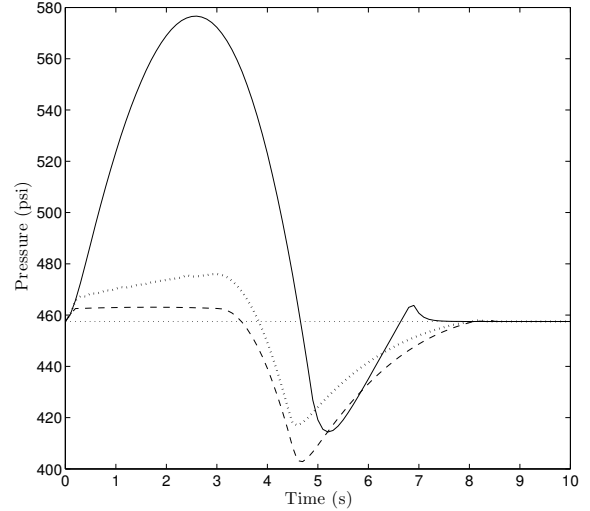


Fig. 7. Steady-state switching using MPC in the absence of plant-model mismatch: system pressure vs. time for “open-loop manually controlled” case (solid line),  $N=1$  (dashed line), and  $N=5$  (dotted line), including pressure set point (horizontal line)

another loop measuring the system pressure while adjusting the retentate valve to maintain the system pressure at the set point. These two loops can be represented as follows:

$$u_{PI}^r = K_r(P_{sys} - P_{sys}^{sp}) + \frac{1}{\tau_r} \int_0^{t_c} (P_{sys} - P_{sys}^{sp}) dt \quad (13)$$

$$u_{PI}^b = K_b(v_b - v_b^{lss}) + \frac{1}{\tau_b} \int_0^{t_c} (v_b - v_b^{lss}) dt \quad (14)$$

Numerous closed-loop simulations were carried out under various PI controller tunings in order to determine the best achievable closed-loop responses. The best achievable closed-loop responses under two different approaches are presented: in the first approach, the PI parameters ( $K_r = -30$ ,  $K_b = 1000$ ,  $\tau_r = -30$ ,  $\tau_b = 1000$ ) were chosen so that the transition is accomplished in a comparable amount of time to the MPC controlled case. It is observed that this case has a poor transient closed-loop performance, due to the presence of large oscillations. It is also noted that the integral term of the PI controller is switched off when the control action is saturated (reaches maximum rate constraint or valve position reaches 100%) to mitigate the effect of integrator wind-up in the closed loop system. In the second tuning approach, the PI parameters ( $K_r = -5$ ,  $K_b = 800$ ,  $\tau_r = -20$ ,  $\tau_b = 500$ ) were chosen in order to conduct the fastest response that does not exhibit any oscillations during the transition between the original and final steady states. In this case, the pressure drops significantly more than any of the MPC cases, and takes a much longer time to converge back to the steady state. The results can be seen in Figs. 8 - 9. The comparisons of MPC with PI demonstrate that

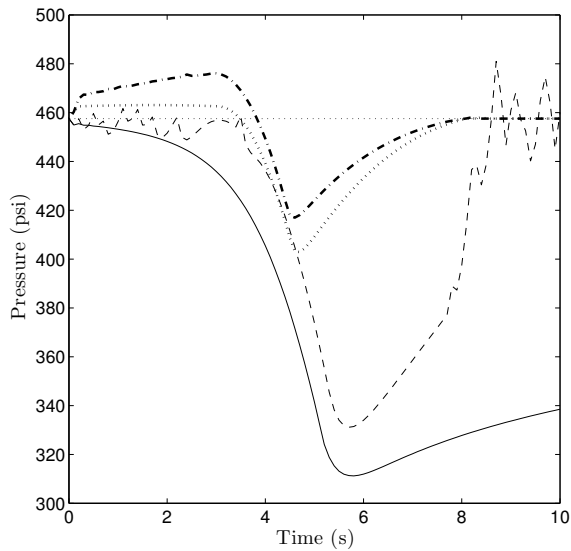


Fig. 8. Steady-state switching using MPC and PI in the absence of plant-model mismatch: pressure vs. time for first PI approach (dashed line), second PI approach (solid line),  $N=1$  (dotted line), and  $N=5$  (dash-dotted line), including pressure set point (horizontal line)

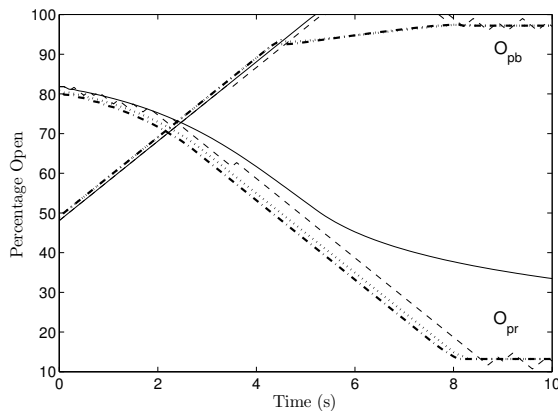


Fig. 9. Steady-state switching using MPC and PI in the absence of plant-model mismatch: valve positions vs. time for first PI approach (dashed line), second PI approach (solid line),  $N=1$  (dotted line), and  $N=5$  (dash-dotted line)

under the MPC formulation, the pressure will deviate from the set point less than the PI controlled case regardless of the PI tuning parameters. The MPC also provides a smoother transition which is accomplished in less time.

In Fig. 10, it can be observed that the values of the cost function decrease with increasing prediction horizon. The cost of these MPC controlled transitions fall between a lower and upper bound; if the pressure weighting in the cost function is set to zero (that is, the pressure is allowed to deviate with no penalty) and transition speed becomes the only factor in switching steady states, then the valves will be opened and closed as fast as possible (equivalent

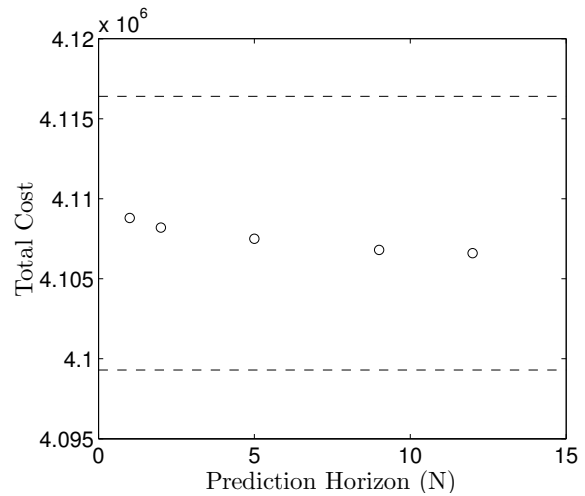


Fig. 10. Total optimization cost vs. prediction horizon with upper and lower bounds based on maximum transition speed

to the "open-loop manually controlled" case). This situation leads to a lower bound on the achievable cost since all of the MPC controlled cases are penalized by pressure fluctuations. In the opposite situation, the MPC controlled cases should perform better than the maximum speed transition (again, the "open-loop manually controlled" case) where the pressure is weighted equivalently to the MPC controlled cases. It can be seen in Fig. 10 that all of the MPC controlled cases at various prediction horizons fall between these two bounds. It is also noted that the magnitudes of the cost function values depend on the individual weighting on each term, but the trend will be independent of term weighting.

## V. CONCLUSIONS

In this work, a model-predictive control strategy for switching between the normal flow operating steady state and the feed flow reversal steady state (where flow into the membrane units is slow enough to prevent water hammer when solenoid valves are closed) was developed. First, a dynamic model of the process was developed as a function of the process parameters, feed concentration, and the bypass/retentate valve resistance values. Using these valve resistance values as control inputs, a non-linear optimization problem was formulated. Solving this optimization through a model-predictive control framework, it was seen that a feedback-based model-predictive controller allowed the system to make the transition between steady states with a much smaller variation in system pressure. The MPC framework was also shown to have a smaller pressure fluctuations and shorter transition time than several well-tuned PI controllers. Non-linear MPC was also shown to be beneficial in the presence of plant-model mismatch. The feedback-based MPC algorithm also improved the speed at which the stream velocities reached the feed flow reversal steady state, decreased the offset between the actual final steady state and the desired final steady state, and damped oscillations in the control action.

## REFERENCES

- [1] A. Abbas. Model predictive control of a reverse osmosis desalination unit. *Desalination*, 194:268–280, 2006.
- [2] A. R. Bartman, C. W. McFall, P. D. Christofides, and Y. Cohen. Model predictive control of feed flow reversal in a reverse osmosis desalination process. *J. Process Contr.*, 19:433–442, 2009.
- [3] R. B. Bird, W. E. Stewart, and E. N. Lightfoot. *Transport Phenomena*, Second Edition. John Wiley and Sons, 2002.
- [4] F.H. Butt, F. Rahman, and U. Baduruthamal. Identification of scale deposits through membrane autopsy. *Desalination*, 101:219–230, 1995.
- [5] P. D. Christofides and N. H. El-Farra. *Control of Nonlinear and Hybrid Process Systems: Designs for Uncertainty, Constraints and Time-Delays*, 446 pages. Springer, New York, 2005.
- [6] N. H. El-Farra, P. Mhaskar, and P. D. Christofides. Hybrid predictive control of nonlinear systems: Method and applications to chemical processes. *Inter. J. Rob. & Non. Contr.*, 14:199–225, 2004.
- [7] N. H. El-Farra, P. Mhaskar, and P. D. Christofides. Uniting bounded control and MPC for stabilization of constrained linear systems. *Automatica*, 40:101–110, 2004.
- [8] S. Hargrove and S. Ilias. Flux enhancement using flow reversal in ultrafiltration. *Separation Science and Technology*, 34:1319–1331, 1999.
- [9] D. Hasson, A. Drak, and R. Semiat. Inception of CaSO<sub>4</sub> scaling on RO membranes at various water recovery levels. *Desalination*, 139:73–81, 2001.
- [10] R.A. Leishear. Dynamic pipe stresses during water hammer: A finite element approach. *Journal of Pressure Vessel Technology*, 129:226–233, 2007.
- [11] Y. Lu, Y. Hu, X. Zhang, L. Wu, and Q. Liu. Optimum design of reverse osmosis system under different feed concentration and product specification. *Journal of Membrane Science*, 287:219–229, 2007.
- [12] C. W. McFall, A. R. Bartman, P. D. Christofides, and Y. Cohen. Control and monitoring of a high-recovery reverse-osmosis desalination process. *Industrial & Engineering Chemistry Research*, 47:6698–6710, 2008.
- [13] C. W. McFall, P. D. Christofides, Y. Cohen, and J. F. Davis. Fault-tolerant control of a reverse osmosis desalination process. In *Proceedings of 8th IFAC Symposium on Dynamics and Control of Process Systems*, volume 3, pages 163–168, Cancun, Mexico, 2007.
- [14] P. Mhaskar, N. H. El-Farra, and P. D. Christofides. Hybrid predictive control of process systems. *AIChE J.*, 50:1242–1259, 2004.
- [15] P. Mhaskar, N. H. El-Farra, and P. D. Christofides. Predictive control of switched nonlinear systems with scheduled mode transitions. *IEEE Trans. Automat. Contr.*, 50:1670–1680, 2005.
- [16] P. Mhaskar, N. H. El-Farra, and P. D. Christofides. Stabilization of nonlinear systems with state and control constraints using Lyapunov-based predictive control. *Syst. & Contr. Lett.*, 55:650–659, 2006.
- [17] R.H. Perry and D.W. Green. *Perry's chemical engineers' handbook*: 7th edition. pages 6–44. McGraw-Hill, 1997.
- [18] N. Pomerantz, Y. Ladizhansky, E. Korin, M. Waisman, N. Daltrophe, and J. Gilron. Prevention of scaling of reverse osmosis membranes by "zeroing" the elapsed nucleation time. part i. calcium sulfate. *Ind. & Eng. Chem. Res.*, 45:2008–2016, 2006.
- [19] A. Rahardianto, J. Gao, C. J. Gabelich, M. D. Williams, and Y. Cohen. High recovery membrane desalting of low-salinity brackish water: Integration of accelerated precipitation softening with membrane RO. *Journal of Membrane Science*, 289:123–137, 2007.
- [20] A. Rahardianto, W. Shih, R. Lee, and Y. Cohen. Diagnostic characterization of gypsum scale formation and control in RO membrane desalination of brackish water. *Journal of Membrane Science*, 279:655–668, 2006.
- [21] M. Uchymiak, A. Rahardianto, E. Lyster, J. Glater, and Y. Cohen. A novel RO ex situ scale observation detector (EXSOD) for mineral scale characterization and early detection. *Journal of Membrane Science*, 291:86–95, 2007.